Earth and Planetary Science Letters 507 (2019) 105–118

Contents lists available at ScienceDirect

Earth and Planetary Science Letters

www.elsevier.com/locate/epsl

Deciphering old moraine age distributions in SE Tibet showing bimodal climatic signal for glaciations: Marine Isotope Stages 2 and 6

Marie-Luce Chevalier [a,*], Anne Replumaz [b]

[a] *Key Laboratory of Deep-Earth Dynamics of Ministry of Natural Resources, Institute of Geology, Chinese Academy of Geological Sciences, 26 Baiwanzhuang Rd, Beijing 100037, People's Republic of China*
[b] *ISTerre, Université Grenoble Alpes, CNRS, Grenoble, France*

ARTICLE INFO

Article history:
Received 27 June 2018
Received in revised form 15 November 2018
Accepted 23 November 2018
Available online 17 December 2018
Editor: A. Yin

Keywords:
SE Tibet
moraine
cosmogenic dating
paleoclimate reconstruction
Marine Isotope Stages
Northern Hemisphere cooling cycles

ABSTRACT

Determining the timing and extent of past glaciations in Tibet is essential to reconstruct regional paleoclimate and understand how atmospheric circulation varies due to the high altitude low latitude Tibetan Plateau. In SE Tibet, geomorphological field observation of glacial deposits shows two main imbricated moraines. We apply statistical analyses to a compilation of eight new ^{10}Be cosmogenic exposure ages from two moraine crests at GMX site and 128 previously published but recalculated exposure ages from 30 additional crests in the region. The results show that ages from the sharpest inner moraines range from 14–25 ka, corresponding to the full range of Marine oxygen Isotope Stage (MIS)-2 (i.e., Last Glacial Maximum, LGM) with less than 2% of older outliers. The outer moraines have a fundamentally different distribution with scattered ages from 10 to 200 ka, obtained using the same method of sampling, dating, and age modeling proven robust for dating the LGM inner moraines, therefore excluding a methodologic artifact. This large scatter prevents the application of any statistical analysis to the age distribution. At a site with well-developed and preserved imbricated moraines (Cuopu), the outer moraine's oldest ages are MIS-6, with the oldest one being at the MIS-6/MIS-7 limit, identical to what is observed in the regional compilation. Following our observations for the LGM moraines where <2% of older outliers are present, the outer moraines in SE Tibet could not be younger than MIS-6. This implies that no glacial advance occurred during MIS-3 which is surprising because MIS-3 moraines have been reported to be the most extensive elsewhere in the Himalayan–Tibetan orogen. Indeed, glaciers are sensitive to both precipitation increase and temperature decrease but whether one factor is prevalent remains debated especially on the Tibetan Plateau. Considering negligible erosion of the boulders, as observed in the field at Cuopu, the most conservative interpretation of our observations is that the true emplacement age of the outer moraines external to the LGM moraines is MIS-6. In that case, glacial advances in SE Tibet correlate with the two coldest periods of the Northern Hemisphere cooling cycles, MIS-2 and MIS-6, indicating that these glaciers are mostly sensitive to a decrease in temperature.

1. Introduction

The Himalayan–Tibetan orogen contains the most glaciated mountains outside of the polar regions, from which all large Asian rivers originate and are essential to the life of billions of people. Studying the timing and extent of past glaciations in the Himalayan–Tibetan orogen provides valuable information for regional paleoclimate reconstruction, climatic patterns, and the role of the high-altitude low latitude Tibetan Plateau in regional and global atmospheric circulation (e.g., Raymo and Ruddiman, 1992; Owen et al., 2005). Indeed, because snow and ice cover have a profound influence on atmospheric circulation (Prell and Kutzbach, 1992), insight on the Tibetan Plateau glaciations is essential to understand past environmental changes which in turn may help predict future climate changes.

Mountain glaciers are extremely sensitive to temperature and precipitation variations and it is still highly debated whether glacial advances on the Tibetan Plateau occurred when temperature decreased or when precipitation increased. Ages of the numerous imbricated moraines in Tibet provide a chronology of successive (less extensive) glacial advances that can be compared with the Northern Hemisphere cooling cycles recorded as Ma-

* Corresponding author.
E-mail addresses: mlchevalier@hotmail.com (M.-L. Chevalier), anne.replumaz@univ-grenoble-alpes.fr (A. Replumaz).

https://doi.org/10.1016/j.epsl.2018.11.033

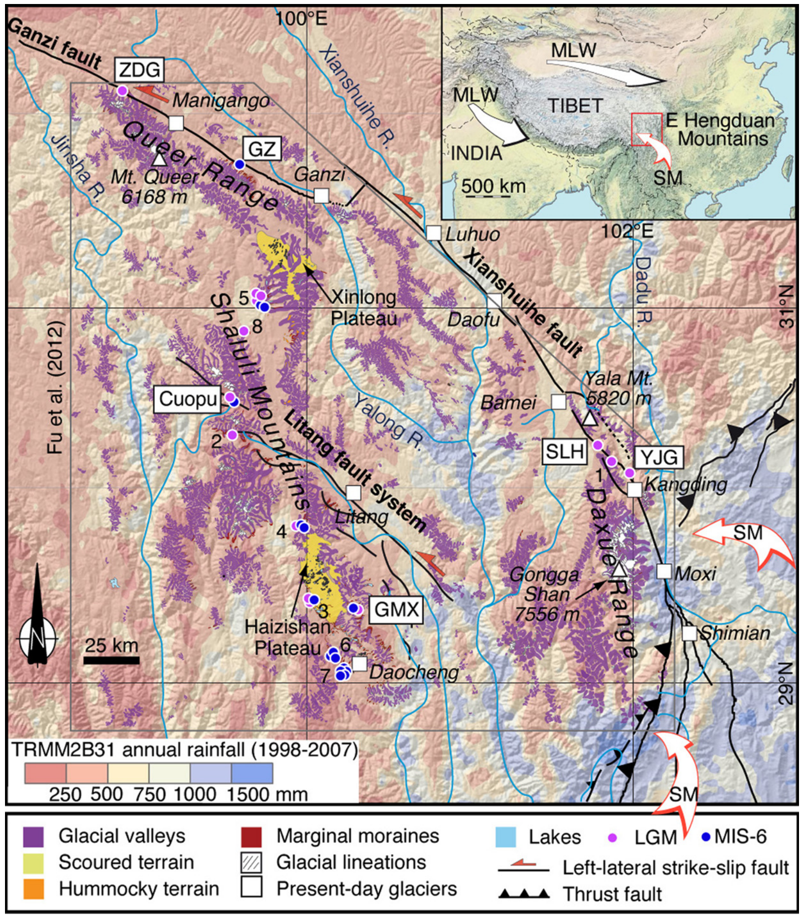

Fig. 1. SE Tibet mapped on a Digital Elevation Model with TRMM precipitation data (pixel size = 4×6 km^2) (Bookhagen and Burbank, 2010). Glacial features from Fu et al. (2012) (within the polygon). Numbers next to colored circles refer to studies in the compilation (Fig. 4), listed in Tables 1 and 2. Study sites from our team in white rectangles. Major towns and peaks are also indicated. Inset shows location of study area within East Asia with dominant climatic systems: mid-latitude Westerlies (MLW) and summer monsoon (SM). (For interpretation of the colors in the figure(s), the reader is referred to the web version of this article.)

rine Isotope Stages (MIS). The two main climatic systems in the Himalayan–Tibetan orogen are the summer monsoon, bringing abundant summer precipitation (as snowfall at high elevation) mostly in the Himalayas as well as the southern and eastern Tibetan Plateau ("monsoon-influenced Tibet"), and the mid-latitude Westerlies, bringing strong winter precipitation to the western regions (Benn and Owen, 1998) (Fig. 1). Throughout the Quaternary, however, the relative importance of these two dominant climatic systems varied significantly, yielding asynchronous glaciations across the orogen (Benn and Owen, 1998; Owen et al., 2005). Many authors found that glacial advances on the Tibetan Plateau during Marine oxygen Isotope Stage (MIS)-3 (∼40 ka) were the most common and the most extensive (e.g., Gillespie and Molnar, 1995; Benn and Owen, 1998; Owen et al., 2005, 2008; Finkel et al., 2003; Chevalier et al., 2011; Wang et al., 2013). These authors argued that at that time, precipitation was more abundant and temperature was warmer (due to insolation increase) than during the Last Glacial Maximum (LGM or MIS-2, ∼20 ka), thus conditions were favorable to glacial advance (Shi et al., 1999). In contrast, the cold and dry climate over the Tibetan Plateau during the LGM (6–9 °C lower and 30–70% less precipitation than present, Shi et al., 1999) was less favorable to glacial advance. In other words, the summer monsoon (with enhanced precipitation) seem to have been the most prevalent factor for glacial advances in most of Tibet. However, in regions such as the western Himalayas and Pamir, where the Westerlies dominate, glaciers were more extensive during the LGM than during MIS-3, in correspondence with the Northern Hemisphere glaciations which reflect global trends in temperature (e.g., Owen and Dortch, 2014; Eugster et al., 2016).

Here, we focus on SE Tibet (Fig. 1), where a series of imbricated moraine systems are characterized by two prominent crests, best illustrated at Cuopu (Fig. 2), our case study published by our team for tectonic purposes (Chevalier et al., 2016). Several studies have used cosmogenic exposure dating of boulders (^{10}Be, ^{26}Al, ^{21}Ne) to date moraines from SE Tibet (e.g., Schäfer et al., 2002; Tschudi et al., 2003; Owen et al., 2005; Wang et al., 2006; Graf et al., 2008; Strasky et al., 2009; Fu et al., 2013a; Chevalier et al., 2016, 2017; Bai et al., 2018) which collectively provide a large dataset to interpret the chronology of regional past glacial advances. The younger, sharper moraine crests located in the inner part of the moraine system have been intensively sampled and dated as LGM. In contrast, few papers present reliable data for the prominent moraines external to the LGM ones (Fu et al., 2013a; Chevalier et al., 2016, 2017). This is mainly due to two problems. The first one is that it can be challenging to find enough suitable samples to date these older deposits due to their poor preservation compared to younger deposits. The second problem is that once dated, the ages of these old moraines are widely scattered, yielding strong uncertainties about their emplacement age, i.e., the deglaciation age, as deglaciation is coeval with moraine abandonment, initiating a period of shape stability and preservation (Fig. 2D).

In this paper, we provide new ^{10}Be exposure ages for eight boulders collected from two moraine crests at Gemuxiang (GMX) site in the Shaluli Mountains, and compile data from 30 addi-

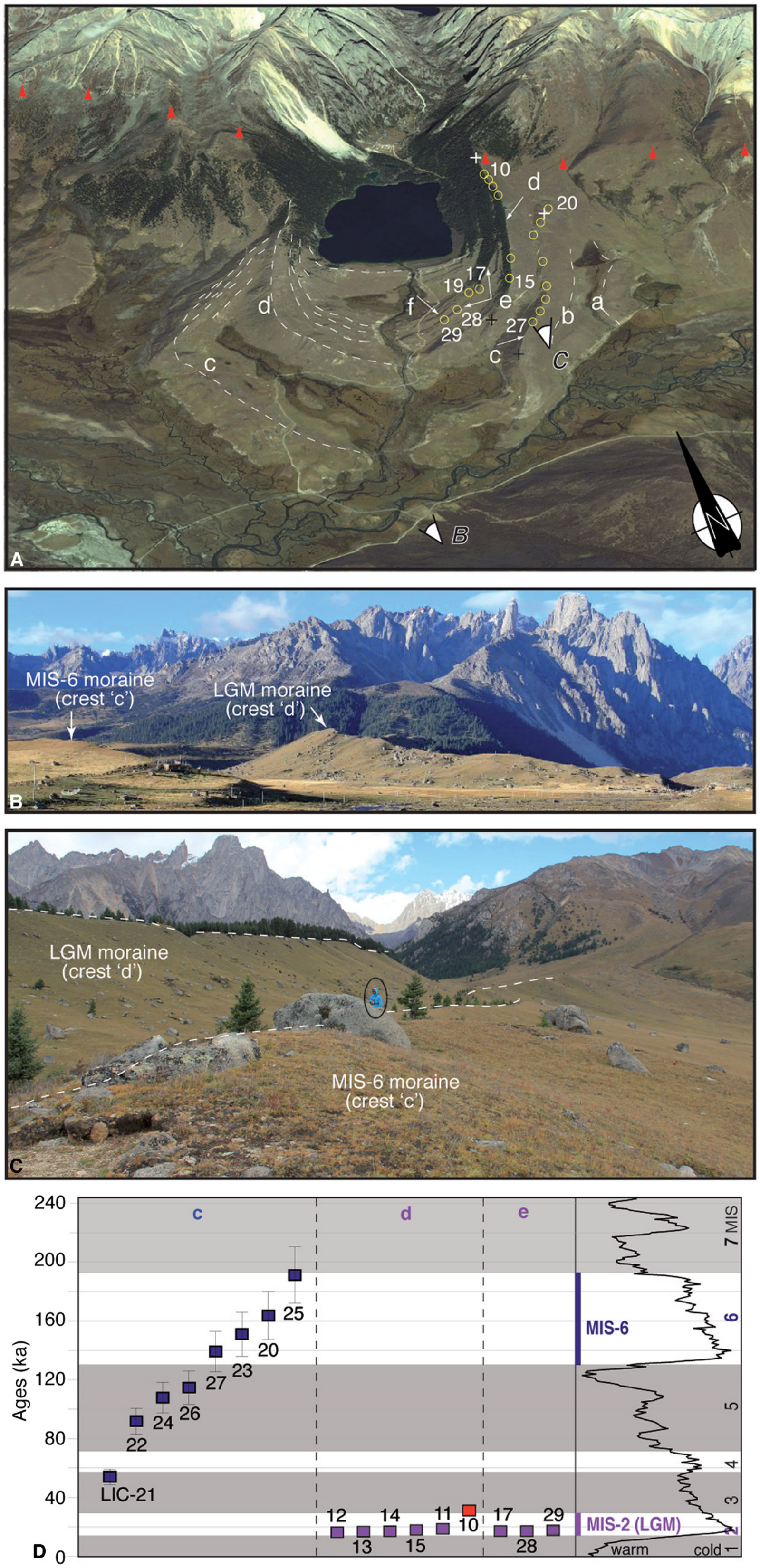

Fig. 2. Cuopu site. (A) Google Earth image of the Cuopu moraine crests 'a–f'. Individual crests highlighted by white dashed lines or open yellow circles showing sample locations and names. Red arrowheads indicate the Cuopu fault. Black and white '+' show the boundaries of the crest profiles (Fig. S9). (B, C) Field views of Cuopu moraine crests 'c' and 'd' (location in A), showing a much sharper and higher crest 'd' than crest 'c', on which boulders are nevertheless present. Person circled for scale. (D) ^{10}Be cosmogenic surface-exposure ages of Cuopu moraines (using the Lal (1991)/Stone (2000) time-dependent model, Tables 1 and 2) with 1σ uncertainty. Red symbol represents the outlier discarded using Peirce's criterion and discussed in the text. To the right, global climatic proxy curve of Lisiecki and Raymo (2005) with gray-shaded sectors showing the Marine oxygen Isotope Stages (MIS).

tional crests located in each of the main mountain ranges of the eastern Hengduan Mountains of SE Tibet. For the younger, inner moraines, a very strong MIS-2 signal with clustered boulder exposure ages spanning the entire stage and with <2% of outliers has been shown in previous studies and compiled here. Exposure ages on boulders from the outer, older moraines are instead highly scattered from ~10 to 200 ka, with the oldest ages ranging from MIS-5 to MIS-7 depending on the moraine (Fu et al., 2013a; Chevalier et al., 2016, 2017). We study here the age distribution of these old moraines, which appears fundamentally different from that of the younger moraines, to try to determine their emplacement age and answer the following questions. Is a large age scatter from 10 to 200 ka representative of the age distribution of the old moraines? Is the scattering of the old moraine ages an artifact due to a problem of methodology or sampling strategy, or is it only due to moraine degradation? Would collecting numerous samples on a few moraine crests or a few samples on numerous crests better reveal the true age of a moraine? Is the oldest age representing a minimum emplacement age or the true emplacement age?

2. Study area and background

The eastern Hengduan Mountains, located in eastern Tibet, comprise several large mountain ranges such as the ~NS-trending Shaluli Mountains, the Queer Range to the north, and the Daxue Range to the east (Fig. 1). This region was extensively glaciated during the Quaternary (Li et al., 1991), evidenced at present by numerous extensive glacial landforms such as erratics, U-shaped valleys, moraines and glacial lakes (mapped in great details by Fu et al., 2012, Fig. 1). Glaciated areas in the Hengduan Mountains were 41 times larger during the LGM than at present (Shi, 2002) but few present-day glaciers remain.

The topography of the massive Shaluli Mountains (which stretch ~450 km, down to Myanmar) is mostly characterized by high-relief mountains with deeply incised valleys, but also by two low-relief granite plateaus, the Haizishan and Xinlong Plateaus (yellow in Fig. 1, Fu et al., 2012). A ~3600 km^2 ice cap (up to 800 m thick) covered the Haizishan Plateau during the Quaternary. Glaciers are absent today because the present-day Equilibrium Line Altitude (ELA) at 5200 m is higher than the peak elevation of the plateau (~4900 m) (Li et al., 1996). Numerous large moraines and U-shaped valleys flank the plateau, long and deep ones in the east versus short, steep and narrow ones in the west (Fu et al., 2013a). The most distinct and extensive moraines correspond to the terminus of former outlet glaciers or the limit of the former Haizishan ice cap margin (Fu et al., 2013a). The Queer Range stretches for ~150 km NW of the city of Ganzi and culminates at 6168 m (Mt. Queer, Fig. 1). It is covered by numerous glaciers and small ice caps at present. The ~150 km-long, currently heavily glaciated Daxue Range is located at the eastern edge of the Tibetan Plateau, where its mean elevation dramatically drops to the Sichuan Basin (from >4000 to ~500 m a.s.l.). The highest peak in the NW Daxue Range (also called Zheduo Range at that location) is Yala Mt. (5820 m), and in the SE Daxue Range, Gongga Shan at 7556 m is the highest peak in eastern Tibet (Fig. 1).

Few ages older than MIS-6 have been reported in SE Tibet for the outermost moraines of the moraine system. Only one cosmogenic exposure age of a boulder at 298.3 ka (MIS-8) assuming zero erosion or ~421 ka (MIS-12) applying an erosion rate of ~1 mm/ka (Wang et al., 2006) and one ESR age of 556.7 ± 62.6 ka (Xu and Zhou, 2009), have been reported at the Kuzhaori moraine complex, formed by an outlet glacier in the SW Haizishan Plateau (#7 in Fig. 1). Its geometry is very similar to that of Cuopu, with two highly degraded outermost moraine crests (Fig. 2A). Finding suitable samples for ^{10}Be cosmogenic exposure dating on these highly degraded moraines has been challenging; only one boulder was found on the two outermost moraines at Cuopu dated at 78 ka (crest 'b'), much younger than the adjacent, younger moraine 'c' at 191 ka, in disagreement with moraine stratigraphy (Chevalier et al., 2016, Fig. 2D). The ages of the oldest moraines in SE Tibet are still unresolved; determining their ages is highly challenging and beyond the scope of this paper. Therefore, we focus our discussion on the two most recent glaciations in SE Tibet which left the two most prominent and preserved imbricated moraines (Fig. 2).

SE Tibet belongs to the monsoon-influenced Tibet region which at places, receives >900 mm/yr of precipitation along the deeply incised, ~NS-trending river valleys (Fig. 1, Bookhagen and Burbank, 2010; Yu et al., 2018). In contrast, central and western Tibet only receive ~200 mm/yr of precipitation, yielding the formation of continental cold glaciers (Shi, 2002). This led Owen et al. (2008) to suggest that glacial advances in SE Tibet respond to both oscillations in the summer monsoon and the Northern Hemisphere cooling cycles (Owen et al., 2008). However, Fu et al. (2013a) suggested that glacial advances in SE Tibet respond only to the Northern Hemisphere cooling cycles, by dating 14 moraine crests and interpreting the deglaciation ages to be Late glacial, MIS-2, MIS-6 or older, plus at least one older glaciation.

3. Methods

To determine the timing of glaciation in SE Tibet, we compile ^{10}Be cosmogenic data reported for 128 moraine boulders and recalculate their exposure ages to obtain a homogeneous dataset. We also add eight new large granite boulder exposure ages from the GMX moraine crests (Fig. S1). The ^{10}Be concentration in the top few centimeters of the largest boulders found on moraine crests (collected using chisel and hammer) can be interpreted as the exposure time of the boulder to incoming cosmic rays (see review papers such as Lal, 1991; Gosse and Phillips, 2001). In the ideal case of the boulder being exposed on the moraine surface since deposition, with no exposure prior to deposition and no rolling or surface erosion since deposition, the exposure time of the boulder will correspond to the age of the moraine. Mineral separation (target mineral is quartz) and quartz cleaning procedure is modified from Kohl and Nishiizumi (1992). We additionally present 59 samples collected on seven moraine crests in the region by our team for tectonic purposes using the same technique, with >8 samples per crest (Chevalier et al., 2016, 2017; Bai et al., 2018). We then compile published regional studies using ^{10}Be exposure dating (Tables 1 and 2), for which more than one boulder per moraine crest older than 13 ka has been collected, and for which all sample and Accelerator Mass Spectrometer (AMS) measurement details needed for exposure age (re)calculations are provided. These criteria exclude several regional studies such as Owen et al. (2005) (too young), Wang et al. (2006) (missing ^{10}Be concentration and AMS standard used, preventing recalculation) and Zhang et al. (2015) (only one sample per crest) as well as some individual moraine crests from studies included in the compilation (Lit 7 in Schäfer et al., 2002; TSO-1 in Graf et al., 2008; K101 in Strasky et al., 2009; crest 'R' in Fu et al., 2013a; Cuopu crests 'b' and 'f' in Chevalier et al., 2016). To discuss which particular MIS glacial stage corresponds to each moraine emplacement, we interpret the boulder age distribution through statistical analysis and compare it with proxy data such as the global stack of benthic δ^{18}O curve of Lisiecki and Raymo (2005).

3.1. ^{10}Be surface-exposure dating and model-age calculation

Several factors may influence the ^{10}Be concentration in the collected samples. Processes like rolling and erosion, as well as shielding, yield ages younger than the moraine emplacement age,

Table 1
Eastern Tibet ^{10}Be inner moraine ages.

Reference	Area	Site name	# in Fig. 1	Sample name	Lat (°N)	Long (°E)	Elev. (m a.s.l.)	Thick-ness (cm)	Density (g/cm^3)	Shielding	^{10}Be (at/g)	err	Standard	Pub-lished age	±	Recalcu-lated age v. 2.3[a]	±	Class[b]
Inner moraines																		
This study	Shaluli Mountains	GMX inner		GMX-7	29.39991	100.27442	4451	5	2.7	0.98	1165380	36174	07KNSTD	/	/	21406	2104	C
				GMX-8	29.40141	100.27604	4434	5	2.7	0.98	1231295	40234	07KNSTD	/	/	22654	2240	
Bai et al. (2018)	Daxue Range	YJG		YJG-1	30.051155	101.928773	3502	5	2.7	0.98	600619	24885	07KNSTD	17652	1749	17652	1749	C
				YJG-2	30.050693	101.928255	3514	5	2.7	0.98	330019	14343	07KNSTD	9834	963	9834	963	
				YJG-3	30.05033	101.928019	3521	5	2.7	0.98	349995	13444	07KNSTD	10386	1011	10386	1011	
				YJG-4	30.049068	101.926476	3562	5	2.7	0.98	368524	16116	07KNSTD	107 08	1154	10708	1154	
				YJG-5	30.053471	101.929568	3475	5	2.7	0.98	619187	23023	07KNSTD	18391	1817	18391	1817	
				YJG-6	30.053703	101.929608	3477	5	2.7	0.98	289736	12886	07KNSTD	8779	871	8779	871	
				YJG-7	30.054779	101.929665	3475	5	2.7	0.98	357576	9963	07KNSTD	10887	1058	10887	1058	
				YJG-8	30.056091	101.930036	3458	5	2.7	0.98	261488	7778	07KNSTD	7954	779	7954	779	
				YJG-9	30.054313	101.929677	3475	5	2.7	0.98	540259	13541	07KNSTD	16217	1542	16217	1542	
		SLH		SLH-1	30.245064	101.717376	4271	5	2.7	0.98	1042537	20881	07KNSTD	20262	1932	20262	1932	B
				SLH-2	30.244629	101.717552	4265	5	2.7	0.98	912145	18738	07KNSTD	17977	1723	17977	1723	
				SLH-3	30.244172	101.716848	4242	5	2.7	0.98	927520	29955	07KNSTD	18465	1825	18465	1825	
				SLH-4	30.243487	101.716246	4241	5	2.7	0.98	847888	19094	07KNSTD	16997	1636	16997	1636	
				SLH-5	30.242491	101.716136	4234	5	2.7	0.98	892433	18594	07KNSTD	17864	1715	17864	1715	
				SLH-6	30.24065	101.716334	4231	5	2.7	0.98	938688	18845	07KNSTD	18766	1797	18766	1797	
				SLH-7	30.239196	101.715253	4229	5	2.7	0.98	1068412	20632	07KNSTD	21209	2021	21209	2021	
				SLH-8	30.239021	101.714604	4223	5	2.7	0.98	1127175	21227	07KNSTD	22346	2125	22346	2125	
				SLH-9	30.238639	101.713716	4224	5	2.7	0.98	1022500	23135	07KNSTD	20337	1941	20337	1941	
				SLH-10[c]	30.238536	101.712427	4224	5	2.7	0.98	1377017	26572	07KNSTD	26766	2572	26766	2572	
Chevalier et al. (2016)	Shaluli Mountains	Cuopu d		LIC-10[c]	30.49535	99.55858	4296	5	2.7	0.98	1721735	55639	07KNSTD	28885	2633	31786	3146	A
				LIC-11	30.49407	99.55808	4292	5	2.7	0.98	978714	33442	07KNSTD	17205	1574	19121	1899	
				LIC-12	30.49258	99.55746	4289	5	2.7	0.98	851187	24420	07KNSTD	15144	1355	16827	1640	
				LIC-13	30.49138	99.55695	4279	5	2.7	0.98	865410	24869	07KNSTD	15460	1384	17162	1673	
				LIC-14	30.48356	99.55147	4206	5	2.7	0.98	850501	24366	07KNSTD	15544	1391	17463	1702	
				LIC-15	30.48244	99.55099	4198	5	2.7	0.98	895273	24223	07KNSTD	16412	1461	18380	1784	
		Cuopu e		LIC-17	30.48278	99.54843	4173	5	2.7	0.98	840820	24251	07KNSTD	15786	1414	17544	1711	A
				LIC-28	30.48145	99.54565	4156	5	2.7	0.98	832941	23078	07KNSTD	15866	1415	17529	1704	
				LIC-29	30.48107	99.54456	4152	5	2.7	0.98	857326	26329	07KNSTD	16284	1469	18036	1770	
Chevalier et al. (2017)	Queer Range	ZDG		ZDG-1	32.109997	98.85129	4144	5	2.7	0.98	741133	23215	07KNSTD	13982	1263	15221	1495	C
				ZDG-2	32.110398	98.851279	4138	5	2.7	0.98	789157	27231	07KNSTD	14878	1362	16173	1607	
				ZDG-3	32.112183	98.851023	4111	5	2.7	0.98	928323	13583	07KNSTD	17431	1501	19043	1796	
				ZDG-4	32.112113	98.851143	4110	5	2.7	0.98	1046391	15848	07KNSTD	19480	1695	21304	2012	
				ZDG-5	32.114641	98.851186	4060	5	2.7	0.98	1087648	16498	07KNSTD	20663	1795	22582	2134	
				ZDG-6	32.115006	98.851970	4049	5	2.7	0.98	1186922	18048	07KNSTD	22531	1952	24566	2323	
				ZDG-7	32.114519	98.852399	4050	5	2.7	0.98	924781	15491	07KNSTD	17863	1564	19529	1849	
				ZDG-8	32.117665	98.852038	4038	5	2.7	0.98	994321	32885	07KNSTD	19321	1761	21018	2080	
				ZDG-9	32.118361	98.852347	4037	5	2.7	0.98	1122651	17144	07KNSTD	21602	1875	23480	2220	
				ZDG-10	32.119341	98.85278	4036	5	2.7	0.98	758114	24012	07KNSTD	15032	1360	16340	1608	
Tschudi et al. (2003)	Daxue Range		1	kan1	30.075	101.813	4240	1.5	2.7	1	916500	58700	S555	12910	1070	16076	1819	C
				kan2	30.075	101.813	4260	1.3	2.7	1	786500	51900	S555	10970	920	13794	1575	
Strasky et al. (2009)	Daxue Range		1	kan102	30.0583	101.8278	4061	3	2.7	0.946	759000	31000	S555	13700	500	15623	1589	A
				kan103	30.0592	101.8263	4071	3	2.7	0.976	851000	38000	S555	14900	600	16782	1734	
				kan104	30.0578	101.8258	4058	3	2.7	0.968	826000	43000	S555	14600	700	16553	1768	
Schäfer et al. (2002)	Shaluli Mountains		2	Lit3	30.3	99.54	4560	2	2.7	1	1108000	92000	S555	13700	1400	16847	2106	A
				Lit4a[c]	30.3	99.54	4560	3	2.7	1	1432000	123000	S555	17700	2000	21525	2736	
				Lit4bc	30.3	99.54	4560	2	2.7	1	1198000	103000	S555	14800	1700	18102	2299	
				Lit5a	30.3	99.54	4610	3	2.7	1	1253000	104000	S555	15100	1600	18608	2327	
				Lit5b	30.3	99.54	4610	3	2.7	1	1247000	101000	S555	15000	1500	18525	2291	
				Lit6	30.3	99.54	4570	3	2.7	1	1248000	101000	S555	15300	1400	18868	2333	
Fu et al. (2013a)	Shaluli Mountains	K	3	TB-09-112	29.42658	100.08858	4461	3	2.7	1	785493	33737	07KNSTD	13000	1200	14339	1471	C
				TB-09-114	29.42657	100.0889	4459	4	2.7	1	772488	27307	07KNSTD	12900	1200	14241	1418	
		J	3	TB-09-13[c]	29.41885	100.01755	4431	2	2.7	1	1047811	34925	07KNSTD	17100	1600	18810	1862	A
				TB-09-12	29.41848	100.01782	4424	2	2.7	1	968473	33026	07KNSTD	16000	1500	17543	1741	
				TB-09-14	29.41877	100.0223	4446	5	2.7	1	900914	34603	07KNSTD	15200	1400	16638	1677	
				TB-09-15	29.41178	100.02077	4424	4.5	2.7	1	901018	35488	07KNSTD	15300	1400	16741	1694	
		N	4	TB-09-76	29.85655	99.95317	4311	4	2.7	1	1260059	46121	07KNSTD	21600	2000	23614	2368	B
				TB-09-75	29.85673	99.95308	4313	3	2.7	1	1184282	33861	07KNSTD	20200	1800	22162	2163	
				TB-09-74	29.85743	99.9531	4339	4	2.7	1	992215	39244	07KNSTD	17100	1600	18750	1899	

(continued on next page)

Table 1 (*continued*)

Reference	Area	Site name	# in Fig. 1	Sample name	Lat (°N)	Long (°E)	Elev. (m a.s.l.)	Thickness (cm)	Density (g/cm^3)	Shielding	^{10}Be (at/g)	err	Standard	Published age	±	Recalculated age v. 2.3[a]	±	Class[b]
Graf et al. (2008)	Shaluli Mountains	Xinlong Plateau	5	TSO-2	31.08667	99.755	4138	2	2.7	0.981	1280000	50000	S555	20100	1000	22855	2313	C
				TSO-3	31.08667	99.755	4138	2	2.7	0.981	1250000	40000	S555	19700	800	22374	2207	
			5	TSO-4	31.08667	99.75667	4150	2	2.7	0.969	1190000	50000	S555	19100	1000	21518	2203	B
				TSO-5	31.08833	99.755	4150	2	2.7	0.981	1080000	30000	S555	16800	700	19443	1891	
				TSO-6	31.08833	99.755	4150	2	2.7	0.981	1150000	30000	S555	18000	700	20615	1996	
			5	TSO-7	31.09	99.76	4156	2	2.7	0.964	1170000	50000	S555	18500	900	21227	2179	B
				TSO-8	31.09	99.75833	4161	3	2.7	0.973	1070000	30000	S555	16800	700	19322	1881	
				TSO-9	31.09333	99.75833	4172	4	2.7	0.954	1310000	40000	S555	20800	800	23555	2313	

Samples GMX were processed at IPG Strasbourg and the ^{10}Be/^{9}Be ratios were measured at CEREGE (NIST SRM4325 (=NIST_27900) with ^{10}Be isotope ratios = 2.79 × 1e−11, equivalent to 07KNSTD). No erosion rate was applied.

[a] Ages calculated with the CRONUS 2.3 calculator using the Lal (1991)/Stone (2000) time-dependent production rate model. ^{10}Be production rate is 4.1 at/g/a.

[b] Class is defined following Heyman (2014), using the reduced Chi-square (χ^2_R) analysis. See text for details.

[c] Outliers from MIS-2 samples rejected using Peirce's criterion (following Blomdin et al., 2016).

while nuclide inheritance, associated with prior exposure, yields ages older than the moraine emplacement age (e.g., Heyman et al., 2011). We corrected for topographic shielding (measured in the field) but not for snow cover due the lack of site-specific or even regional data. The vegetation cover is in general minimal at the study sites so that its shielding is negligible. We recalculated the exposure ages from the compilation using the CRONUS calculator version 2.3 (Balco et al., 2008) (Tables 1 and 2) with the widely used Lal (1991)/Stone (2000) time-dependent scaling model. First, we assume zero erosion and take the calculated apparent ages as minimum ages. Second, we discuss the influence of both the erosion of the boulder surface and of the moraine matrix, which results in rounding and smoothing of the moraine crest with time and gradual or episodic exhumation of initially buried boulders, both of which result in boulder exposure ages that are younger than the moraine emplacement age. We also attempt to sort the boulders according to their ages or their position along the moraine crests discussed here (Figs. S1–S7) to determine whether a correlation exists between boulder sizes, their position on the crest and their ages.

One may examine the influence of erosion on boulder exposure ages by applying a rate of 1 to 3 mm/ka, as deduced from nearby studies, using the height difference between a quartzite knob and its granite boulder surface (Graf et al., 2008) or between glacially-polished bedrock underneath and next to an erratic boulder (Wang et al., 2006). Applying a 1 mm/ka erosion rate yields a negligible apparent exposure age increase of <2% for 20 ka samples (inner moraines) and a more substantial age increase of 22% for our oldest age on the outer moraine at Cuopu at 191 ka (MIS-6/MIS-7 boundary) (becoming 234 ka, MIS-7). A 3 mm/ka erosion rate increases 20 ka sample ages by <5%, which is still negligible, and 191 ka ages become saturated in CRONUS, therefore deeply affecting old ages and shifting the MIS to a much older period, possibly older than the oldest ages ever measured in SE Tibet.

The erosion rate of 1 mm/ka applied to the outermost moraines, which then belong to MIS-12 (Wang et al., 2006), seems a reasonable maximum rate. In any case, since no direct measurement of present-day or past erosion rate exists for our region of interest, we consider that adding such unconstrained erosion rate leads to high uncertainties. Therefore, we choose to assume zero erosion when calculating the ages in CRONUS and we interpret the continuous distribution of older moraine ages as reflecting erosion of the moraine matrix and of the boulder surface, which we will discuss in detail using field observations.

3.2. Statistical analysis of the age distribution

In order to statistically test whether outliers are present in a single moraine age distribution of more than two samples, we apply Peirce's criterion (Peirce, 1852) following Blomdin et al. (2016). We then apply the reduced Chi-square (χ^2_R) analysis to test whether a single moraine age distribution is well-clustered following Heyman (2014), who suggested the following classification: Class A defines moraines having well-clustered ages and a $\chi^2_R \leq 2$, class B defines moraines having moderately-clustered ages and a χ^2_R >2 as well as a mean exposure age >85% of the oldest exposure age, and class C defines moraines having poorly-clustered ages, i.e., which do not fit into classes A nor B. For class A moraines, one may take the mean age to represent the deglaciation age while for classes B and C moraines, the oldest age best represents the minimum deglaciation age (Heyman, 2014), with a true emplacement age that could be much older (e.g., Heyman et al., 2011; Fu et al., 2013a). Moraine crests with only two samples (four such crests falling in the inner moraine group and one crest falling in the outer moraine group, Tables 1 and 2) are automatically labeled as class C. Since class C moraines all have $\chi^2_R > 2$

Table 2
Eastern Tibet ^{10}Be outer moraine ages.

Reference	Area	Site name	# in Fig. 1	Sample name	Lat (°N)	Long (°E)	Elev. (m a.s.l.)	Thickness (cm)	Density (g/cm^3)	Shielding	^{10}Be (at/g)	err	Standard	Published age	±	Recalculated age v. 2.3[a]	±	Class[b]
Outer moraines																		
This study	Shaluli Mountains	GMX outer		GMX-1	29.40762	100.29071	4327	5	2.7	0.98	5498779	92658	07KNSTD	/	/	97932	9460	C
				GMX-2	29.406	100.28741	4373	5	2.7	0.98	3283714	63626	07KNSTD	/	/	57266	5503	
				GMX-3	29.40563	100.28514	4391	5	2.7	0.98	8391046	135637	07KNSTD	/	/	141776	13830	
				GMX-4	29.40364	100.28136	4437	5	2.7	0.98	1578967	34031	07KNSTD	/	/	28254	2709	
				GMX-5	29.40181	100.27934	4456	5	2.7	0.98	3059703	95972	07KNSTD	/	/	50132	4970	
				GMX-6	29.39977	100.27621	4479	5	2.7	0.98	1696368	52070	07KNSTD	/	/	29556	2908	
Chevalier et al. (2017)	Queer Range	GZ		GZ-1	31.728473	99.5791	4037	5	2.7	0.98	2750064	28421	07KNSTD	47905	4137	53515	5061	C
				GZ-2	31.728449	99.579118	4037	5	2.7	0.98	1649108	20622	07KNSTD	30602	2633	33432	3155	
				GZ-3	31.728569	99.577947	4046	5	2.7	0.98	1206399	18693	07KNSTD	22856	1979	25144	2379	
				GZ-4	31.728672	99.577378	4050	5	2.7	0.98	5184287	40987	07KNSTD	92631	8088	100743	9616	
				GZ-5	31.728657	99.576364	4059	5	2.7	0.98	441636	10919	07KNSTD	8590	758	9633	927	
				GZ-6	31.728642	99.575935	4064	5	2.7	0.98	653355	12464	07KNSTD	12750	1109	14154	1345	
				GZ-7	31.728826	99.573827	4086	5	2.7	0.98	3542070	33703	07KNSTD	61868	5351	67858	6434	
				GZ-8	31.731137	99.580608	3998	5	2.7	0.98	3452762	31801	07KNSTD	63033	5455	69157	6557	
				GZ-10B	31.731971	99.581753	3981	5	2.7	0.98	2649745	47960	07KNSTD	47481	4159	52984	5073	
				GZ-11	31.731592	99.581215	3992	5	2.7	0.98	5111314	105669	07KNSTD	94061	8425	102129	9955	
				GZ-12	31.731267	99.580712	3999	5	2.7	0.98	4100957	86575	07KNSTD	74770	6662	82500	8010	
				GZ-13	31.731492	99.581215	3993	5	2.7	0.98	2069945	37339	07KNSTD	37951	3313	41116	3924	
Fu et al. (2013a)	Shaluli Mountains	I	3	TB-09-100	29.39033	99.99083	4506	4.5	2.7	1	496252	18903	07KNSTD	8100	800	9010	905	C
				TB-09-102	29.40253	99.99217	4512	4	2.7	1	4741402	111113	07KNSTD	68100	6100	75352	7345	
				TB-09-101	29.39737	99.99385	4499	3	2.7	1	11011911	246145	07KNSTD	156000	14100	174383	17380	
		L	4	TB-09-128	29.86533	99.92715	4504	2	2.7	1	1626225	57542	07KNSTD	24600	2300	26925	2690	C
				TB-09-129	29.86075	99.93195	4485	3.5	2.7	1	6380809	168216	07KNSTD	92300	8300	100778	9964	
				TB-09-130	29.85378	99.93718	4440	3	2.7	1	9213369	197387	07KNSTD	131200	11800	146446	14461	
		M	4	TB-09-79	29.8461	99.96567	4455	4	2.7	1	6664799	115631	07KNSTD	97600	8600	106532	10323	B
				TB-09-77	29.8476	99.96508	4444	5	2.7	1	6964769	245159	07KNSTD	102600	9600	112235	11450	
				TB-09-78	29.84657	99.96537	4450	3	2.7	1	7421466	269125	07KNSTD	106700	10100	116804	11976	
		O	5	TB-09-64	31.03253	99.7082	4379	5	2.7	1	7104294	218367	07KNSTD	104900	9700	114929	11556	B
				TB-09-65	31.03225	99.70828	4373	2	2.7	1	8647890	190875	07KNSTD	123100	11100	136257	13441	
				TB-09-63	31.03112	99.7082	4369	3	2.7	1	8947551	208913	07KNSTD	128700	11600	143144	14190	
				TB-09-62	31.0313	99.70825	4371	3	2.7	1	9387503	184244	07KNSTD	135000	12100	151038	14870	
		P	5	TB-09-58	31.0239	99.72135	4233	3	2.7	1	5551872	131718	07KNSTD	88100	7900	96910	9504	C
				TB-09-56	31.02635	99.72408	4258	3	2.7	1	8212087	182648	07KNSTD	124800	11200	138256	13650	
				TB-09-57	31.026	99.7237	4250	4	2.7	1	8192745	204919	07KNSTD	126000	11400	139810	13908	
		F	6	TB-08-27	29.1753	100.10678	4056	2	2.7	1	4523014	191634	07KNSTD	80500	7700	89329	9314	C
				TB-08-26	29.17457	100.1077	4067	3	2.7	1	4563242	297350	07KNSTD	81500	8900	90373	10477	
				TB-08-28	29.17543	100.10657	4053	1	2.7	1	6745227	166465	07KNSTD	116200	10500	127952	12679	
		G	6	TB-08-31	29.17777	100.09523	4064	1.5	2.7	1	1334108	37865	07KNSTD	25500	2300	27599	2695	C
				TB-08-30	29.17765	100.09519	4062	2	2.7	1	3191645	95884	07KNSTD	57300	5200	62705	6209	
				TB-08-29	29.17771	100.09525	4062	3	2.7	1	5294601	135234	07KNSTD	95900	8700	103471	10214	
		H	6	TB-08-03	29.20897	100.093	4231	3	2.7	1	3192983	121110	07KNSTD	51400	4800	57963	5892	C
				TB-08-02	29.20897	100.093	4215	3	2.7	1	4980105	190271	07KNSTD	82600	7800	91497	9390	
				TB-08-01	29.20672	100.09058	4216	3	2.7	1	6247289	274133	07KNSTD	102300	10000	111947	11812	
		A	7	TB-08-10	29.12415	100.22163	3871	1	2.7	1	2084297	65233	07KNSTD	40300	3700	43598	4314	C
				TB-08-18	29.12553	100.22237	3892	2	2.7	1	7827647	164708	07KNSTD	149200	13500	166352	16494	
		B	7	TB-09-119	29.12847	100.21805	3919	3	2.7	1	6479634	133499	07KNSTD	121300	10800	133932	13158	B
				TB-09-121	29.12948	100.2182	3929	4	2.7	1	7176619	295393	07KNSTD	135300	13100	150681	15878	
				TB-09-120	29.12907	100.21812	3924	2	2.7	1	8012489	262649	07KNSTD	150700	14200	167618	17196	
		C	7	TB-08-34	29.11897	100.20985	3867	2	2.7	1	4360926	126357	07KNSTD	85700	7800	94700	9422	B
				TB-08-33	29.11893	100.20963	3864	2	2.7	1	4915283	102300	07KNSTD	96400	8600	105271	10273	
				TB-08-32	29.11882	100.20948	3864	2	2.7	1	5534562	120464	07KNSTD	106900	9600	117197	11497	
		D	7	TB-08-24	29.1236	100.21198	3931	3	2.7	1	2700506	84991	07KNSTD	50600	4600	56992	5661	C
				TB-08-23	29.12342	100.21185	3928	3	2.7	1	2877747	105209	07KNSTD	54700	5100	61107	6185	
				TB-08-22	29.12288	100.21147	3916	3	2.7	1	6230089	194946	07KNSTD	117200	10900	128952	13036	

(continued on next page)

Table 2 (*continued*)

Reference	Area	Site name	# in Fig. 1	Sample name	Lat (°N)	Long (°E)	Elev. (m a.s.l.)	Thick-ness (cm)	Density (g/cm^3)	Shielding	^{10}Be (at/g)	err	Standard	Pub-lished age	±	Recalcu-lated age v. 2.3[a]	±	Class[b]
		E	7	TB-08-19	29.12353	100.20957	3904	2	2.7	1	5571308	97268	07KNSTD	105700	9300	115681	11238	B
				TB-08-20	29.12295	100.20913	3904	5	2.7	1	5812484	147660	07KNSTD	112400	10200	123090	12207	
				TB-08-21	29.12258	100.20882	3904	4	2.7	1	6513632	238263	07KNSTD	123800	11700	136959	14131	
		Q	8	TB-09-04	30.86763	99.6377	4063	3	2.7	1	7124691	114697	07KNSTD	120100	10600	132554	12898	C
				TB-09-02	30.86815	99.64302	4043	3	2.7	1	8984509	256643	07KNSTD	155100	14400	173051	17539	
				TB-09-03	30.86843	99.64295	4036	3	2.7	1	10472668	272273	07KNSTD	183600	17000	200740	20336	
Chevalier et al. (2016)	Shaluli Mountains	Cuopu c		LIC-20	30.48948	99.55989	4246	5	2.7	0.98	9062644	125465	07KNSTD	145435	13046	164018	16026	C
				LIC-21	30.48852	99.55858	4243	5	2.7	0.98	3030450	53503	07KNSTD	47938	4195	54878	5252	
				LIC-22	30.48642	99.55575	4222	5	2.7	0.98	5006816	91206	07KNSTD	83079	7366	92715	8968	
				LIC-23	30.48384	99.55453	4199	5	2.7	0.98	8242716	120469	07KNSTD	134627	12050	151657	14790	
				LIC-24	30.48206	99.55309	4193	5	2.7	0.98	5901635	89037	07KNSTD	98276	8697	108716	10497	
				LIC-25	30.48031	99.55197	4186	5	2.7	0.98	10284488	141577	07KNSTD	173075	15669	191525	18842	
				LIC-26	30.47865	99.54978	4190	5	2.7	0.98	6299673	97123	07KNSTD	104612	9284	115526	11180	
				LIC-27	30.47812	99.54898	4181	5	2.7	0.98	7603770	112322	07KNSTD	124729	11130	139833	13600	

Samples GMX were processed at IPG Strasbourg and the ^{10}Be/^{9}Be ratios were measured at CEREGE (NIST SRM4325 (=NIST_27900) with ^{10}Be isotope ratios = 2.79 × 1e−11, equivalent to 07KNSTD). No erosion rate was applied.

[a] Ages calculated with the CRONUS 2.3 calculator using the Lal (1991)/Stone (2000) time-dependent production rate model. ^{10}Be production rate is 4.1 at/g/a.

[b] Class is defined following Heyman (2014), using the reduced Chi-square (χ^2_R) analysis. See text for details.

here, the oldest age represents the minimum moraine deglaciation age (Heyman, 2014).

4. Results: the Gemuxiang (GMX) site

The Gemuxiang (GMX) moraines are located in the southern Shaluli Mountains (Fig. 1), ~65 km south of the city of Litang and ~40 km north of the city of Daocheng, where its former outlet glacier was flowing northeastward from the Haizishan Plateau (Fu et al., 2012, 2013b and Fig. 1). The GMX moraines are ~3 km-long and consist of more than four distinct crests, with several preserved frontal crests inside which a large glacial lake remains (Fig. 3). The crests are steep (5°) and high (~200 m), with the outer crest covered by small bushes and the inner crests covered by trees on the inward-facing slopes (Fig. 3). Eight samples from the largest granite boulders (with coarse, friable grains) were collected on the eastern crests (Figs. 3B and S1). The two samples from the inner crest are similar at 21.4 ± 2.1 and 22.7 ± 2.2 ka (Figs. 4, S8 and Table 1) and correspond to the LGM. The six ages from the outer crest range from 28.3 ± 2.7 to 141.8 ± 13.8 ka. Applying Peirce's criterion to this dataset shows that the outer moraine is class C, i.e., poorly-clustered so that the oldest age represents the minimum deglaciation age, which is MIS-6. We will further discuss and compare this exposure age distribution with that of the regional compilation, to better evaluate the significance of the scattered age distribution, considering that statistical analyses on such large age scatter are irrelevant.

5. Review of existing data

5.1. The case study site with imbricated moraines: the Cuopu site

The Cuopu moraines are located in the northern Shaluli Mountains (Fig. 1). They are one of the most extensive and preserved imbricated moraines in SE Tibet due to their emplacement in a wide sedimentary basin opened by the Cuopu normal fault exhuming the adjacent range (Chevalier et al., 2016). There was only one main glacier flowing over ~10 km from the highest local peak, avoiding interaction between adjacent moraines. A series of imbricated moraines are observed around the glacial lake (Fig. 2), with the two oldest crests ('a' and 'b') being preserved outwards to the east thanks to the former right-lateral strike-slip component of the Cuopu fault (Fig. 2A) (Chevalier et al., 2016). These crests are highly degraded with no boulder remaining on crest 'a' and only one boulder remaining on crest 'b' (Chevalier et al., 2016). The sharpest and highest moraine (crest 'd') is covered by numerous large granite boulders and trees on the inward-facing slopes (Fig. 2B, C). Closer to the lake, younger moraines are also covered by large granite boulders and are sharp-crested but lower, with multiple sub-crests hard to distinguish from one another due to their close proximity (among which crest 'e' in Fig. 2A). Farther from the lake, the prominent moraine 'c' surrounds moraine 'd' but is sub-rounded and much lower (Fig. 2B, C). It is also covered by numerous large granite boulders and short grass (Fig. 2C).

Seventeen samples have been collected from crests 'c, d, e' (Chevalier et al., 2016) (Fig. 2D and Tables 1 and 2). Applying Peirce's criterion and using the reduced Chi-square analysis, the youngest moraine 'e' shows no outlier and can be classified as class A (Fig. 4), thus the average age of 17.7 ± 0.3 ka ($n = 3$) represents the deglaciation age. The sharpest and highest crest 'd', with ages ranging between 17.2 ± 1.7 and 19.2 ± 1.9 ka, can also be classified as class A excluding one outlier (sample LIC-10 at 31.8 ± 3.1 ka), so that the mean age of 17.8 ± 0.9 ka ($n = 5$) is taken to represent the deglaciation age. Therefore, moraines 'e' and 'd' are LGM with only one older outlier. In contrast the outer prominent moraine 'c'

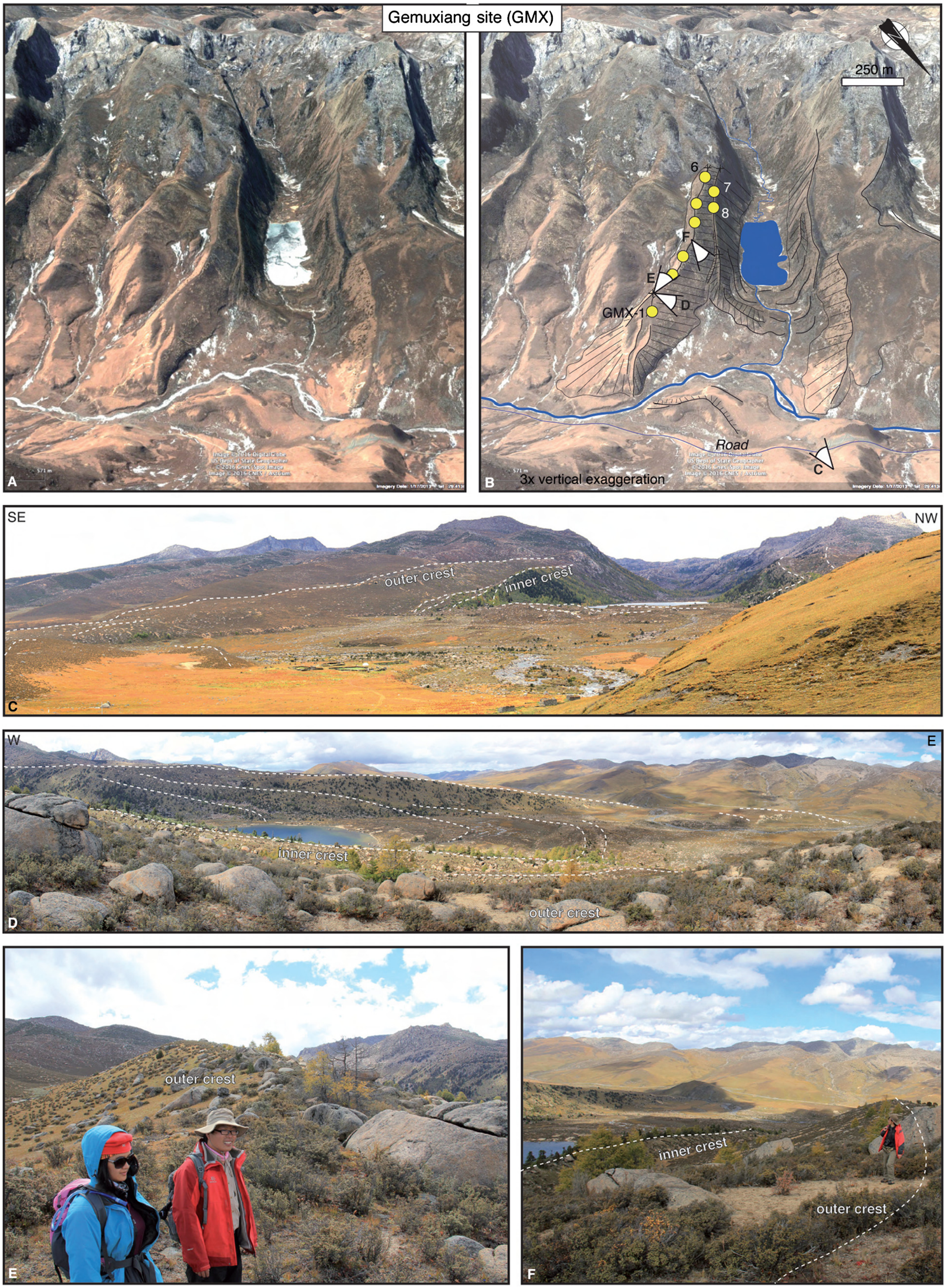

Fig. 3. Gemuxiang (GMX) site. (A, B) Site GMX on Google Earth images (29.39991°N–100.27442°E) showing samples location as well as location of photos C–F. Black '+' show the boundaries of the crest profiles (Fig. S9). (C) View looking upstream at the GMX moraine complex and the Haizishan Plateau. (D) View from the eastern outer crest, looking at the inner, frontal and western crests. (E, F) Close-up photos of the crests where one can see boulder sizes and vegetation cover.

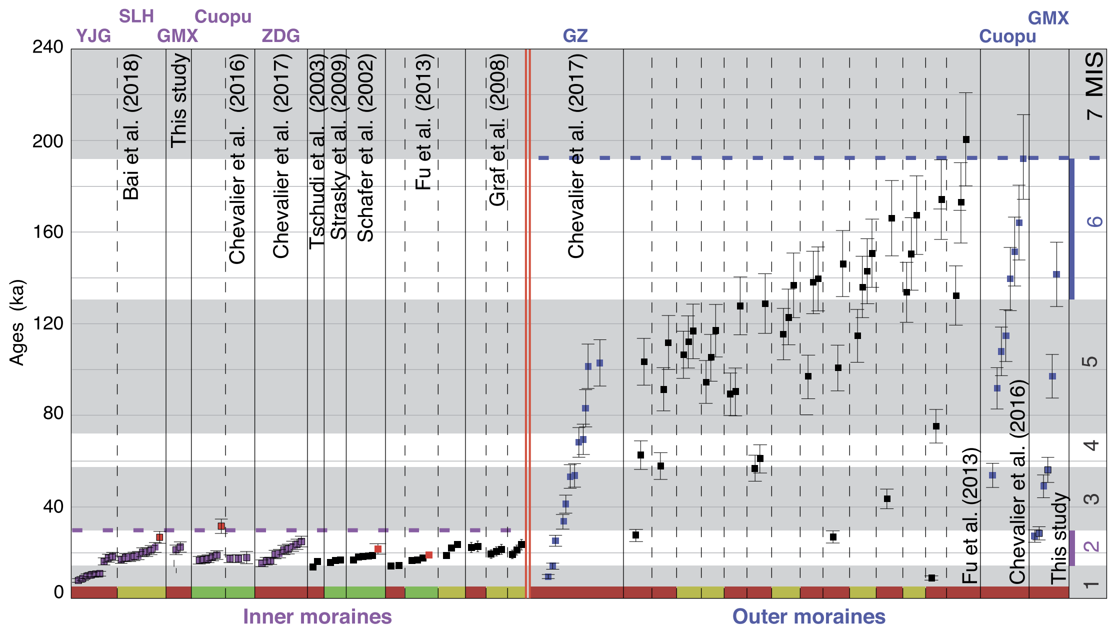

Fig. 4. Compilation of ^{10}Be moraine ages (with 1σ uncertainties) from SE Tibet (purple and blue symbols refer to samples from our team), recalculated using CRONUS v2.3 (Tables 1 and 2). Vertical dashed lines separate the different crests within each study. The inner moraines clearly show a LGM (MIS-2) signal. Outer moraine ages are scattered, reflecting moraines' degradation, with the oldest ages being MIS-6, interpreted as the deglaciation age. Red symbols represent outliers rejected by Peirce's criterion and discussed in the text. Colors at the bottom of the graph refer to well-clustered (green, class A), moderately-clustered (yellow, class B) and poorly-clustered (red, class C) moraine ages, obtained using the reduced Chi-square (χ^2_R) analysis (Heyman, 2014). See text for details. Site abbreviation names refer to Yangjiagou (YJG), Gemuxiang (GMX), Ganzi (GZ), Zhuqing (ZDG) and Selaha (SLH) moraines. The latter two sites are described in detail in the Supplemental material and Fig. S10.

has a completely different age distribution, with ages widely scattered between 54.9 ± 5.3 and 191.5 ± 18.8 ka ($n = 8$), i.e., mostly falling within MIS-5 and MIS-6, with only the youngest sample being MIS-3 and the oldest one being MIS-6/MIS-7 considering uncertainties (Fig. 2D).

5.2. The Ganzi (GZ) moraine

The Ganzi (GZ) moraines are located in the SE Queer Range, ∼40 km NW of the city of Ganzi (Fig. 1). This part of the range still has several small glaciers and numerous large U-shaped valleys and moraines that extend ∼4 km north of the range. This sampling was originally done for tectonic purposes because the GZ moraine is offset by the Ganzi fault by ∼800 m (Chevalier et al., 2017). The most extensive GZ moraines have a smoother topography than the more recent moraines upstream (Fig. 5D) and are covered by grass and small bushes (Fig. 5E), as well as small granite boulders (Fig. S4). Chevalier et al. (2017) collected 12 samples from the western crest whose ages are widespread and 'continuous' from 9.6 ± 0.9 to 102.1 ± 10 ka, with the oldest age corresponding to MIS-5 (Fig. 4 and Table 2).

5.3. The Yangjiagou (YJG) moraine: a degraded LGM moraine

In order to further discuss the influence of erosion on moraine age distributions, we present here in detail a peculiar inner moraine, the Yangjiagou (YJG) moraine. It is located in the NW Daxue Range, in a steep environment along the deeply entrenched Kangding valley, ∼6 km NW of the city of Kangding (Fig. 1). This part of the range does not have contemporary glaciers but numerous glacial lakes and young moraines abound towards the highest peaks, resembling a scoured terrain. However, few moraines are well-defined and are present as low as the YJG moraine. It has previously been studied by several authors who suggested a qualitative age only. Allen et al. (1991) were the first ones to draw attention to the YJG moraine by conducting field work and remote sensing on the active Xianshuihe fault (Fig. 1), whose Selaha fault branch cuts and left-laterally offsets the YJG moraine crest by ∼80 m (Bai et al., 2018).

The YJG moraine is <2 km-long, and is covered by large granite boulders and small bushes (Fig. 5C). Allen et al. (1991) inferred an age of 13 ka, arguing that the moraine must have formed at the peak of glaciation in order to become stable enough to start being offset by the Selaha fault, and Chen et al. (2016) inferred an age of 18 ka. Bai et al. (2018) collected nine samples along the crest and quantitatively determined exposure ages that range from 8.0 ± 0.8 to 18.4 ± 1.8 ka (Figs. 4, S8 and Table 1). No outlier is statistically rejected and YJG is class C with the oldest age being LGM.

5.4. Other study sites in SE Tibet

Numerous studies have sampled the inner moraines in SE Tibet (Schäfer et al., 2002; Tschudi et al., 2003; Graf et al., 2008; Strasky et al., 2009; Fu et al., 2013a; Chevalier et al., 2016, 2017; Bai et al., 2018) (Figs. 4, S8 and Table 1). In contrast, few cosmogenic datasets are available for the outer moraines: one presented in this paper (GMX outer, $n = 6$), two published by our team (Cuopu crest 'c' in Chevalier et al., 2016 with $n = 10$; GZ in Chevalier et al., 2017 with $n = 12$), and one dataset published by Fu et al. (2013a) with 42 samples on 14 moraine crests, but with only 2–4 samples per crest. The three sites studied by our team are presented in detail in this paper (Figs. 2, 3 and 5), while details about each site from Fu et al. (2013a) can be found in the publication.

Surprisingly, the large dataset of Fu and collaborators (the only other study of older moraines using ^{10}Be in SE Tibet), show that their age compilation with only 2–4 samples per moraine on numerous moraine crests ($n = 14$) is similar to our dense sampling ($n = 6$–10) on three crests (Cuopu, GZ and GMX). When taken together, the compilation of all outer moraine ages shows continuous ages between mostly MIS-5 and MIS-6 with two ages at the MIS-6/MIS-7 limit, i.e., 68% of the outer moraine ages fall within MIS-5 and MIS-6 ($n = 46$) with only 1/3 being MIS-4 or younger ($n = 22$, i.e. 32%).

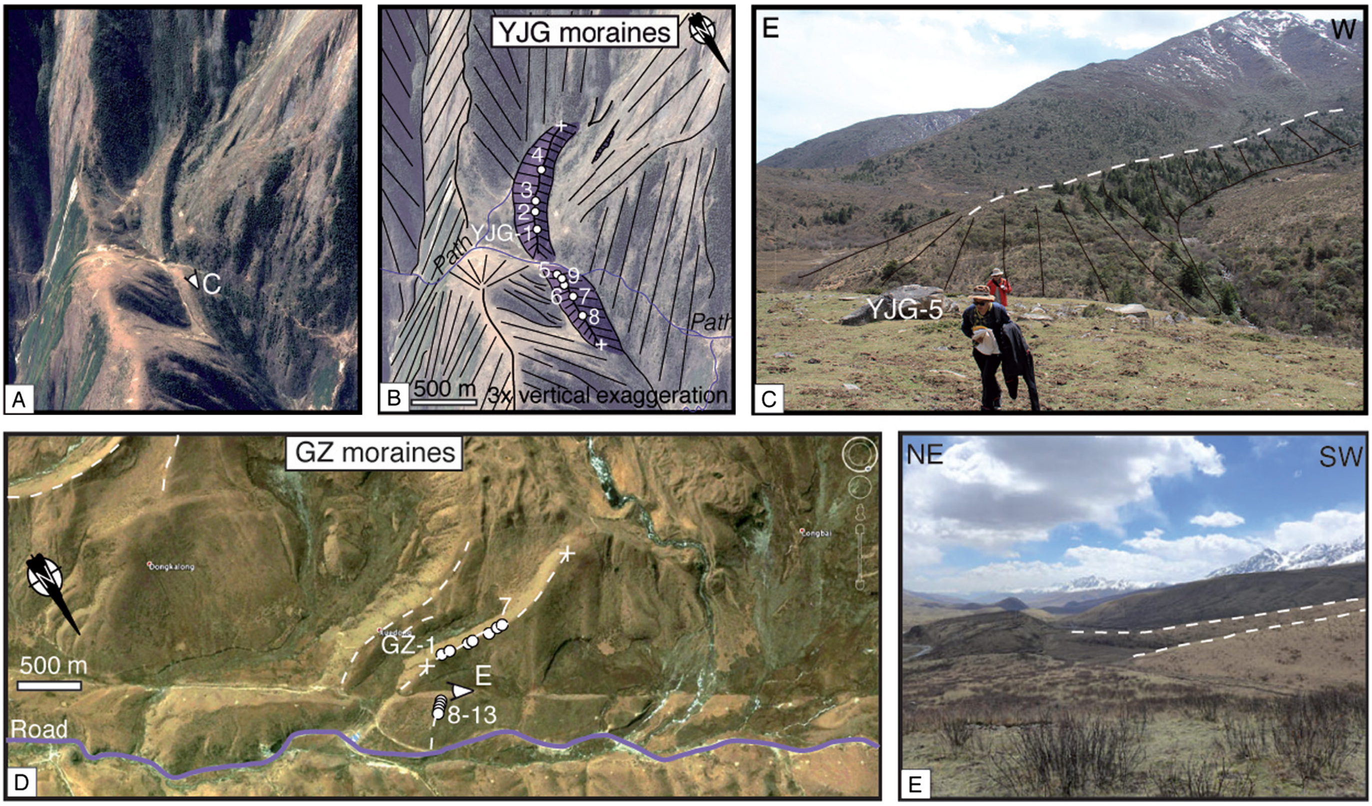

Fig. 5. YJG and GZ sites. (A, B) Site Yangjiagou (YJG) on Google Earth images showing the samples location as well as location of photo C, modified from Bai et al. (2018). (C) Photo looking upstream at the YJG crest. Note the large boulder (YJG-5) and people for scale. (D) Ganzi (GZ) site on Google Earth image with Chevalier et al.'s (2017) samples location on the most extensive moraine crest. Location of photo E is indicated. (E) View of GZ moraine from the location of samples GZ-8-13 with the crests in white dashed lines. White '+' show the boundaries of the crest profiles (Fig. S9).

6. Discussion and interpretation

6.1. Clustered age distribution of inner moraines: LGM emplacement

All data from the compilation of SE Tibet inner moraines, except YJG, show a homogeneous pattern with ages spanning the full range of MIS-2 (LGM), i.e., 14 to 25 ka, with <2% of older outliers (Figs. 4 and S8). If each moraine age distribution is taken individually, four outliers out of 59 samples are statistically rejected (red in Figs. 4 and S8) while if taken as a single distribution, only one outlier (LIC-10) out of 59 samples is statistically rejected. This low percentage of outliers (<2%) older than MIS-2 indicates that there is no significant nuclide inheritance affecting the boulders emplaced with the LGM moraines. Taking the average age of all samples except the four outliers discarded by Peirce's criterion ($n = 55$) or the average age of all samples except that outside of MIS-2 yields similar values at 19.0 ± 2.6 ka (purple Gaussian peak in Fig. 6D) or 19.2 ± 2.8 ka, respectively. This clustering of ages shows that our method of sampling, dating and interpreting is robust, yielding reliable MIS-2 ages for the inner moraines and suggests that the degradation process on the inner moraines located on the flat plateau is negligible, so that collecting three samples per moraine crest may be sufficient to estimate their emplacement age.

At YJG, the age distribution is quite different from that of the other inner moraines, with the three oldest ages corresponding to the LGM and the six younger ages clustering between 8.0 ± 0.8 and 10.9 ± 1.1 ka (Figs. 4 and S8), i.e., with a bimodal Probability Density Function (PDF) at the LGM and at ~10 ka (pink in Fig. 6D). This moraine is much smaller than any of the other moraines (Fig. 6A) and is not located on the flat Tibetan plateau (>4000 m a.s.l. like all the other moraines from the compilation) but along its steep edge (3500 m a.s.l.), in a region with more precipitation prograding northwestward in the deep valley of Kangding (Fig. 1, Yu et al., 2018). Therefore we suggest that the young peak at YJG reveals a more degraded morphology, in agreement with its peculiar location. An alternative scenario in which the youngest peak would represent the actual deglaciation age (Younger Dryas) and the older ages would be outliers (inherited samples reworked from upstream) is unlikely, because in that case, the number of old outliers would be much higher (33%) than what we observe for the compilation of inner moraines (<2%). We conclude that the age distribution of the YJG moraine with numerous young ages could be the signature of a highly degraded moraine, and we compare it to the age distribution of the outer moraines (dark blue in Fig. 6C).

6.2. Continuous age distribution of outer moraines: MIS-6 emplacement

The ages at our case study site of Cuopu crest 'c', between MIS-5 and MIS-6 and with one at the MIS-6/MIS-7 limit, show a scattered and continuous distribution suggesting that the sampling is dense enough ($n = 8$) to be representative. This age distribution is in agreement with that of the regional compilation which is made of one regional study obtained on 14 moraine crests with only 2–4 samples per crest (Fu et al., 2013a). Therefore, despite the fact that a sampling strategy with few samples is inconclusive for just one moraine, when viewed as a whole, the compilation of few ages from numerous crests as done by Fu et al. (2013a) reveals a distribution appearing overall representative of the regional signal (Fig. 4). Such distribution with widely scattered ages prevents the application of statistical tests, as done on the LGM moraines.

Assuming a synchronous glaciation episode over SE Tibet and considering an emplacement mode of the old outer moraines sim-

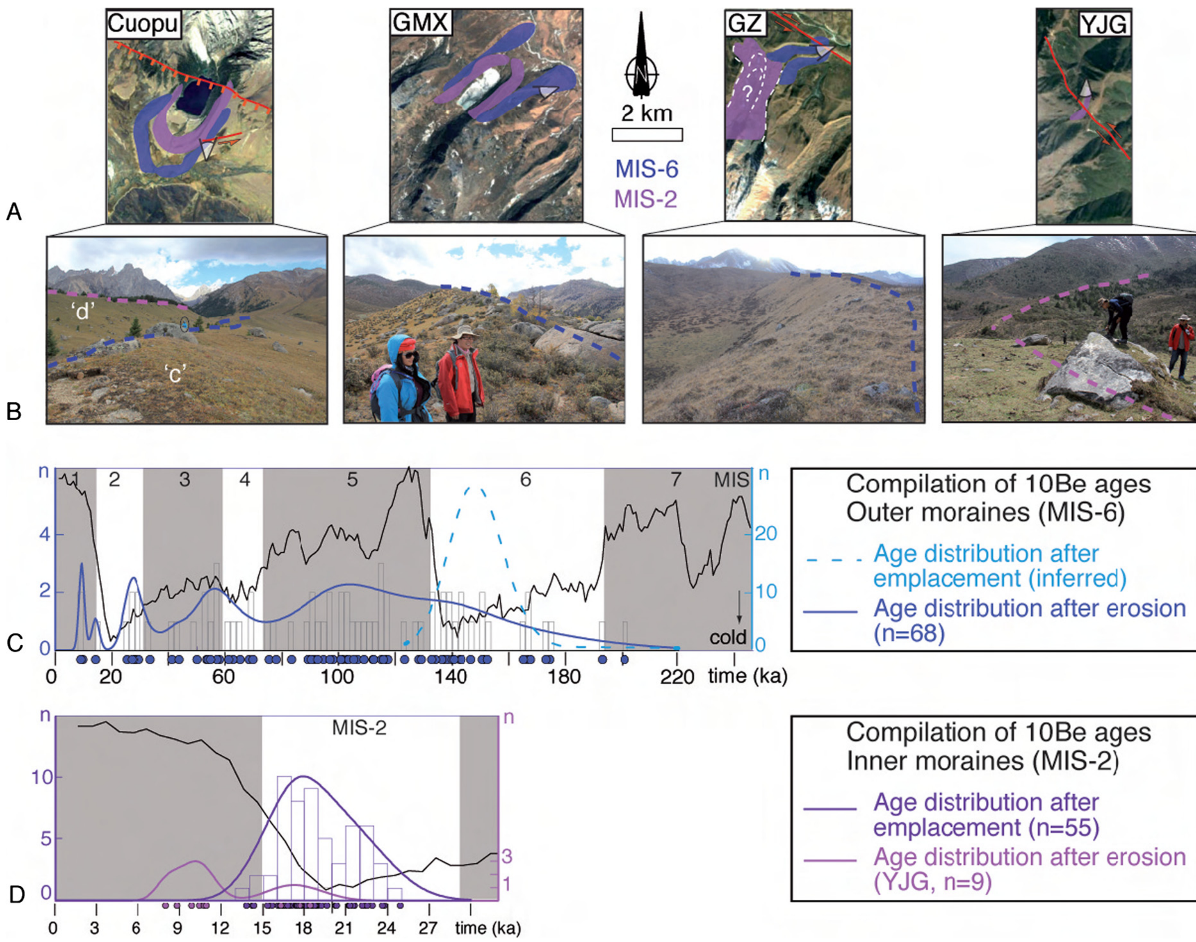

Fig. 6. Statistical analyses of moraine ages. (A) Comparison of moraine extent for each site plotted at the same scale and with the same orientation. Pink tones show MIS-2 (LGM) crests and blue tones show MIS-6 crests. Question mark denotes age uncertainty for inner moraine at GZ, inferred to be LGM. The red lines depict active left-lateral faults plus a normal fault at Cuopu. (B) Corresponding photos of each moraine crest showing boulder sizes (which are much smaller at GZ) and vegetation cover. Photo locations shown by eye symbols in A. (C) Probability density functions (PDF) of outer moraine ^{10}Be ages from the compilation in Fig. 4 with the dashed curve representing what the distribution might have looked like after a moraine's emplacement (light blue), while the actual curve (dark blue) reflects degradation. Climatic curve of Lisiecki and Raymo (2005) in black (cold pointing down). (D) PDF of inner moraine ^{10}Be ages from the compilation in Fig. 4 except YJG (purple) and of YJG only (pink), showing the different age distribution: a Gaussian centered on the emplacement age of the moraine for the former, versus a broad distribution with two peaks reflecting degradation at YJG due to its location at the edge of the Tibetan Plateau near the deep valley of Kangding, for the latter. Data from the compilation can be found in Tables 1 and 2.

ilar to that of the LGM inner moraines with few old outliers due to negligible inheritance ($<2\%$), no emplacement age younger than MIS-6 is compatible with a low percentage of old outliers.

6.3. Erosion of outer moraines

The continuous age distribution during MIS-6 and MIS-5 revealed by the compilation and best illustrated at Cuopu crest 'c' (Figs. 2D and 4) is consistent with the age distribution expected from a moraine affected by continuous diffusional degradation. The most important process is the degradation of the matrix, leading to an increasing degree of moraine crest rounding with age, i.e., with its outer position (Fig. 4). This allows exhumation of the boulders which then gradually appear younger. This process has been slow in the studied region, not yet affecting the inner LGM moraines which show no degradation yet (sharp crest) and clustered ages representing the emplacement age, except for the highly degraded YJG moraine.

For the YJG moraine, the degradation mechanism most likely occurs through erosion of the matrix due to heavy rain on the edge of the plateau (Fig. 1), yielding exhumation of buried boulders which then yield exposure ages younger than the moraine emplacement age, but nevertheless preserving a cluster of ages representative of the LGM emplacement age (Fig. 6D). According to us, the most conservative interpretation of our observations is that some of the original boulders may also be preserved on some well-preserved outer moraines such as Cuopu. Indeed, numerous boulders are still present on Cuopu crest 'c' (Fig. 2), showing no obvious sign of erosion of their surfaces such as knobs or holes. In that case we suggest that some boulders can still record the true emplacement age of the moraine, despite erosion of the matrix. Therefore, we favor this more conservative estimate in which the oldest ages at MIS-6 are representative of the moraine emplacement. Indeed, that the error bar largely overlaps with a MIS-6 age may allow to consider the oldest age at the MIS-6/MIS-7 limit as belonging to MIS-6.

On the contrary, at the GMX site, we noticed in the field that sample grains are coarser, more friable, and relatively easily eroded off the boulders and deposited at their foot compared to the other sites (reddish versus gray granite boulders, respectively, Figs. S1–S7). This observation is indicative of erosion of the boulder surfaces once they are exhumed out of the matrix, which is not observed at Cuopu. We suggest that the age range at GMX outer, which is similar to that of Cuopu crest 'c' with the oldest age being MIS-6 (Fig. 4) but with more numerous younger ages, is due to higher boulder degradation in addition to matrix degradation.

At GZ, only small boulders are present on the outer crest (Fig. S4). The GZ crest is higher ($\sim$20 m), steeper ($\sim$7–10°, because deposited in the piedmont) and sharper than Cuopu crest 'c' (a few meters high at places, ∼1–3° slope, deposited in a wide flat basin), which may allow boulders first brought to the surface by exhumation to roll downhill (Figs. 2, 5, 6 and S9) so that the oldest calculated boulder exposure age is younger than the oldest exposure age in the compilation. Indeed despite a dense sampling, the GZ ages show a different distribution than that of the other outer moraines, with no age older than MIS-5 and young ages as young as 9.6 ± 0.9 ka (MIS-1), which account for the most numerous young samples in the compilation (Fig. 4). We speculate that additional dating would lead to the same age distribution.

In summary, the large scatter (from 10 to 200 ka) in the age distribution of the moraines external to the LGM moraines, appears to be the norm rather than the exception (Fig. 4). This pattern is not due to a problem of methodology, nor is it due to a problem of sampling since the LGM moraines' age distribution is clustered. Such a distribution with widely scattered ages requires a dense sampling of each crest to be representative of one age distribution, and prevents the application of statistical tests, as done on the LGM moraines. Our team's dense sampling on three crests allows us to discuss the degradation of the various outer moraines, which we interpret to have experienced similar erosion of the matrix but different degrees of erosion on the boulder surfaces. Indeed, Cuopu shows no clear sign of boulder erosion and has numerous MIS-6 ages, GMX outer clearly shows signs of boulder erosion and has only one MIS-6 age, and GZ has no more large boulder on its crest and no more MIS-6 ages. As no erosion rate of the boulders could be measured or precisely estimated at Cuopu, the most conservative interpretation of our observations is that negligible erosion of the boulders occurred at Cuopu, a well-preserved moraine deposited in a flat sedimentary basin, and that in that case the oldest age of the distribution best represents the true emplacement age, being MIS-6.

The fact that a dense sampling of few crests (such as done by our team) reveals a similar age distribution to that obtained from collecting few samples on numerous crests (as done by Fu et al., 2013a) suggests that the outer moraines sampled in the region by the latter team have experienced similar paleoclimate conditions. However, building of a strong database to precisely understand how past climate might have varied in space and time throughout a region can only be conducted following the former approach of sampling numerous boulders on a moraine crest, as advocated by Chevalier et al. (2011). In addition, having more data per crest allows to better assess the complexity of the erosion processes reflected as a large scatter in the age distribution.

6.4. Regional and global climatic correlations

Considering the MIS-6 oldest ages as representative of the emplacement age, our analysis of the outer moraines' age distribution external to the LGM moraines in SE Tibet shows that they coincide with the major ice peaks of the Northern Hemisphere cooling cycles (Fig. 6C). Plotting the three outer moraine sites discussed in detail here, at the same scale and with the same direction (Fig. 6A) reveals no influence of glacial valley orientation compared to possible dominant wind direction. The position of these moraines out of the present-day influence of the monsoon, i.e., away from the deeply entrenched valleys, receiving <500 mm/yr of rainfall (Fig. 1, Yu et al., 2018; Bookhagen and Burbank, 2010) suggests a weak influence of monsoonal precipitation in the local glacial history, which helps preserve moraines ≥MIS-6. However sites located in areas under the monsoon's influence, such as the YJG site in the Daxue Range, where present-day precipitation is >900 mm/yr (Fig. 1, Yu et al., 2018), are highly degraded with a large age spread from 8 to 18 ka, atypical of LGM moraines for which ages generally cluster well (pink vs purple in Fig. 6D).

6.5. Absence of MIS-3 glaciation in SE Tibet

The compilation of 136 ^{10}Be boulder exposure ages and interpreted moraine ages from SE Tibet shows that the main glaciations (with the best preserved moraines) are bimodal with peaks at LGM and MIS-6 (Fig. 6C). Indeed, that glacial advances occurred during the LGM, a major cooling episode (e.g., Clark et al., 2009), has been extremely well-documented. Climatic conditions during MIS-6 being highly similar to that during the LGM, both stages corresponding to the largest ice peaks of the global ice volume (Fig. 6C), a MIS-6 glacial advance is the most conservative hypothesis (Fig. 6C). Importantly, the fact that no MIS-3 glaciation is found in the compilation is surprising, especially since it has been shown to be the most common and the most extensive glaciation on the Tibetan Plateau due to abundant precipitation and warm temperature compared to the LGM (e.g., Benn and Owen, 1998; Finkel et al., 2003). This indicates that glaciers from SE Tibet respond more sensitively to a decrease in temperature (e.g., Schäfer et al., 2002; Graf et al., 2008; Strasky et al., 2009; Fu et al., 2013a) than an increase in precipitation (e.g., Benn and Owen, 1998; Finkel et al., 2003). In other words, we suggest that glaciers in SE Tibet were less influenced by the summer monsoon than by the Northern Hemisphere cooling cycles.

7. Conclusion

While most people study moraines that are LGM or younger, few people attempt to study older moraines, due to the difficulty in finding suitable material (large boulders may not be present anymore), the much more degraded morphology of old moraines compared to younger ones, and especially because of the difficulty in interpreting the large age scatter of old moraines and assigning deglaciation ages. Here, using the results from our previous work on tectonics using moraines as offset geomorphic markers, and combining them with other studies from SE Tibet using ^{10}Be cosmogenic data on moraines external to the LGM inner moraines, our interpretation suggests bimodal moraine ages at MIS-2 and MIS-6 but with very different age distributions. Samples from the inner, sharper moraines span MIS-2 with very few older outliers ($<2\%$). In contrast, the outer moraine ages are widely scattered (10–200 ka). The spread of old moraine ages does not reflect a problem of sampling or methodology proved valid for the younger moraines, but rather, that erosion is responsible for moraine's degradation, yielding ages younger than the deglaciation age. Such degradation is more intense when the moraine crests are steeper or the boulders are more friable, leading to more numerous young ages, and ultimately to the loss of the true deglaciation age. In this case, the oldest age of the distribution best represents the minimum deglaciation age which is MIS-6. This implies that no glacial advance occurred during MIS-3, in contrast to the rest of the Himalayan–Tibetan orogen where they have been found to be the most extensive.

We argue that at Cuopu, our case study where moraines deposited in a flat basin are well-preserved with no clear sign of boulder erosion, the most conservative interpretation is that the oldest age of the distribution best represents the true emplacement age, being MIS-6. In that case, the two main imbricated moraines observed in SE Tibet are MIS-2 and MIS-6 corresponding to the two largest ice peaks of the global ice volume. They respond to the Northern Hemisphere cooling cycles, suggesting that glaciers in SE Tibet are more sensitive to changes in temperature than changes in precipitation.

Acknowledgements

This project was conducted under the auspices of the Natural National Science Foundation of China NSFC [41672210, 41672211], the China Geological Survey CGS [DD20160022], the Basic Outlay of Scientific Research Work from the Institute of Geology, CAGS [J1528], as well as the Cai Yuanpei program [27968UC] of the China Scholarship Council/French Ministry of Education. We are very grateful to the Observatoire des Sciences de l'Univers de Grenoble (OSUG) for hosting MLC as a visiting Professor to write this paper. We want to thank Arjen Stroeven as well as an anonymous reviewer for their very thorough reviews and suggestions which improved our manuscript.

Appendix A. Supplementary material

Supplementary material related to this article can be found online at https://doi.org/10.1016/j.epsl.2018.11.033.

References

Allen, C.R., Luo, Z., Qian, H., Wen, X., Zhou, H., Huang, W., 1991. Field study of a highly active fault zone: the XSF of southwestern China. Geol. Soc. Am. Bull. 103, 1178–1199.

Bai, M., Chevalier, M.-L., Pan, J., Replumaz, A., Leloup, P.H., Métois, M., et al., 2018. Southeastward increase of the late Quaternary slip-rate of the Xianshuihe fault, eastern Tibet. Geodynamic and seismic hazard implications. Earth Planet. Sci. Lett. 485, 19–31. https://doi.org/10.1016/j.epsl.2017.12.045.

Balco, G., Stone, J.O., Lifton, N.A., Dunai, T.J., 2008. A complete and easily accessible means of calculating surface exposure ages or erosion rates from ^{10}Be and ^{26}Al measurements. Quat. Geochronol. 3 (3), 174–195. https://doi.org/10.1016/j.quageo.2007.12.001.

Benn, D.I., Owen, L.A., 1998. The role of the Indian summer monsoon and the mid-latitude westerlies in Himalayan glaciation: review and speculative discussion. J. Geol. Soc. 155, 353–363.

Blomdin, R., Stroeven, A.P., Harbor, J.M., Lifton, N.A., Heyman, J., Gribenski, N., et al., 2016. Evaluating the timing of former glacier expansions in the Tian Shan: a key step towards robust spatial correlations. Quat. Sci. Rev. 153, 78–96. https://doi.org/10.1016/j.quascirev.2016.07.029.

Bookhagen, B., Burbank, D.W., 2010. Toward a complete Himalayan hydrological budget: spatiotemporal distribution of snowmelt and rainfall and their impact on river discharge. J. Geophys. Res. 115, F03019. https://doi.org/10.1029/2009JF001426.

Chen, G., Xu, X., Wen, X., Chen, Y., 2016. Late Quaternary slip-rates and slip-partitioning on the southeastern Xianshuihe fault system, Eastern Tibetan Plateau. Acta Geol. Sin. 90, 537–554.

Chevalier, M.-L., Hilley, G., Tapponnier, P., Van Der Woerd, J., Liu-Zeng, J., Finkel, R.C., et al., 2011. Constraints on the late Quaternary glaciations in Tibet from cosmogenic exposure ages of moraine surfaces. Quat. Sci. Rev. 30 (5–6), 528–554. https://doi.org/10.1016/j.quascirev.2010.11.005.

Chevalier, M.-L., Leloup, P.H., Replumaz, A., Pan, J., Liu, D., Li, H., et al., 2016. Tectonic-geomorphology of the Litang fault system, SE Tibetan Plateau, and implication for regional seismic hazard. Tectonophysics 682, 278–292. https://doi.org/10.1016/j.tecto.2016.05.039.

Chevalier, M.-L., Leloup, P.H., Replumaz, A., Pan, J., Métois, M., Li, H., 2017. Temporally constant slip rate along the Ganzi fault, NW Xianshuihe fault system, eastern Tibet. Geol. Soc. Am. Bull. 130 (3–4), 396–410.

Clark, P.U., Dyke, A.S., Shakun, J.D., Carlson, A.E., Clark, J., Wohlfarth, B., et al., 2009. The Last Glacial Maximum. Science 325, 710–714. https://doi.org/10.1126/science.1172873.

Eugster, P., Scherler, D., Thiede, R.C., Codilean, A.T., Strecker, M.R., 2016. Rapid Last Glacial Maximum deglaciation in the Indian Himalaya coeval with midlatitude glaciers: new insights from ^{10}Be-dating of ice-polished bedrock surfaces in the Chandra Valley, NW Himalaya. Geophys. Res. Lett. 43, 1589–1597. https://doi.org/10.1002/2015GL066077.

Finkel, R.C., Owen, L.A., Barnard, P.L., Caffee, M.W., 2003. Beryllium-10 dating of Mount Everest moraines indicates a strong monsoon influence and glacial synchroneity throughout the Himalaya. Geology 31, 561–564.

Fu, P., Heyman, J., Hättestrand, C., Stroeven, A.P., Harbor, J.M., 2012. Glacial geomorphology of the Shaluli Shan area, southeastern Tibetan Plateau. J. Maps 8 (1), 48–55.

Fu, P., Stroeven, A.P., Harbor, J.M., Hättestrand, C., Heyman, J., Caffee, M.W., et al., 2013a. Paleoglaciation of Shaluli Shan, southeastern Tibetan Plateau. Quat. Sci. Rev. 64, 121–135.

Fu, P., Harbor, J.M., Stroeven, A.P., Hattestrand, C., Heyman, J., Zhou, L., 2013b. Glacial geomorphology and paleoglaciation patterns in Shaluli Shan, the southeastern Tibetan Plateau – evidence for polythermal ice cap glaciation. Geomorphology 182, 66–78. https://doi.org/10.1016/j.geomorph.2012.10.030.

Gillespie, A., Molnar, P., 1995. Asynchronous maximum advances of mountain and continental glaciers. Rev. Geophys. 33, 311–364.

Gosse, J., Phillips, F., 2001. Terrestrial in situ cosmogenic nuclides: theory and application. Quat. Sci. Rev. 20, 1475–1560.

Graf, A.A., Strasky, S., Zhao, Z.Z., Akar, N., Ivy-Ochs, S., Kubik, P.W., et al., 2008. Glacier extension on the eastern Tibetan Plateau in response to MIS 2 cooling, with a contribution to ^{10}Be and ^{21}Ne methodology. In: Strasky, S. (Ed.), Glacial Response to Global Climate Changes: Cosmogenic Nuclide Chronologies from High and Low Latitudes. University of Bern, Bern, pp. 77–110. PhD thesis, ETH Zürich.

Heyman, J., 2014. Paleoglaciation of the Tibetan Plateau and surrounding mountains based on exposure ages and ELA depression estimates. Quat. Sci. Rev. 91, 30–41. https://doi.org/10.1016/j.quascirev.2014.03.018.

Heyman, J., Stroeven, A.P., Harbor, J.M., Caffee, M.W., 2011. Too young or too old: evaluating cosmogenic exposure dating based on an analysis of compiled boulder exposure ages. Earth Planet. Sci. Lett. 302 (1–2), 71–80.

Kohl, C.P., Nishiizumi, K., 1992. Chemical isolation of quartz for measurement of in situ produced cosmogenic nuclides. Geochim. Cosmochim. Acta 56, 3583–3587.

Lal, D., 1991. Cosmic ray labeling of erosion surfaces: in situ nuclide production rates and erosion models. Earth Planet. Sci. Lett. 104, 429–439.

Li, B., Li, J., Cui, Z., Zheng, B., Zhang, Q., Wang, F., Zhou, S., Shi, Z., Jiao, K., Kang, J., 1991. Quaternary Glacial Distribution Map of Qinghai–Xizang (Tibet) Plateau. Science Press, Beijing. Map scale 1:3,000,000 (in Chinese).

Li, J., Feng, Z., Zhou, S., 1996. Quaternary glacial remnants in Hengduan Shan. In: Li, J. (Ed.), Glaciers in Hengduan Shan. Science Press, Beijing, pp. 157–173 (in Chinese).

Lisiecki, L.E., Raymo, M.E., 2005. A Pliocene–Pleistocene stack of 57 globally distributed benthic δ^{18}O records. Paleoceanography 20 (1). https://doi.org/10.1029/2004PA001071.

Owen, L.A., Finkel, R.C., Barnard, P.L., Ma, H.Z., Asahi, K., Caffee, M.W., et al., 2005. Climatic and topographic controls on the style and timing of Late Quaternary glaciation throughout Tibet and the Himalaya defined by ^{10}Be cosmogenic radionuclide surface exposure dating. Quat. Sci. Rev. 24 (12–13), 1391–1411.

Owen, L.A., Caffee, M.W., Finkel, R.C., Seong, Y.B., 2008. Quaternary glaciation of the Himalayan–Tibetan orogen. J. Quat. Sci. 23 (6–7), 513–531.

Owen, L.A., Dortch, J.M., 2014. Nature and timing of Quaternary glaciation in the Himalayan–Tibetan orogen. Quat. Sci. Rev. 88, 14–54. https://doi.org/10.1016/j.quascirev.2013.11.016.

Peirce, B., 1852. Criterion for the rejection of doubtful observations. Astron. J. 2, 161–163.

Prell, W.L., Kutzbach, J.F., 1992. Sensitivity of the Indian monsoon to forcing parameters and implications for its evolution. Nature 360, 647–652.

Raymo, M.E., Ruddiman, W.F., 1992. Tectonic forcing of late Cenozoic climate. Nature 359, 117–122.

Schäfer, J.M., Tschudi, S., Zhao, Z., Wu, X., Ivy-Ochs, S., Wieler, R., et al., 2002. The limited influence of glaciations in Tibet on global climate over the past 170000 yr. Earth Planet. Sci. Lett. 194, 287–297.

Shi, Y., 2002. Characteristics of late Quaternary monsoonal glaciation on the Tibetan Plateau and in East Asia. Quat. Int. 97–98, 79–91.

Shi, Y., Liu, X., Li, B., Yao, T., 1999. A very strong summer monsoon event during 30–40 ka BP in the Qinghai–Xizang (Tibet) plateau and its relation to precessional cycle. Chin. Sci. Bull. 44 (20), 1851–1857.

Stone, J.O., 2000. Air pressure and cosmogenic isotope production. J. Geophys. Res. 105, 23753–23759.

Strasky, S., Graf, A.A., Zhao, Z., Kubik, P.W., Baur, H., Schlüchter, C., et al., 2009. Late Glacial ice advances in southeast Tibet. J. Asian Earth Sci. 34 (3), 458–465.

Tschudi, S., Schäfer, J.M., Zhao, Z., Wu, X., Ivy-Ochs, S., Kubik, P.W., et al., 2003. Glacial advances in Tibet during the Younger Dryas? Evidence from cosmogenic ^{10}Be, ^{26}Al, and ^{21}Ne. J. Asian Earth Sci. 22 (4), 301–306.

Wang, J., Raisbeck, G., Xu, X., Yiou, F., Bai, S., 2006. In situ cosmogenic ^{10}Be dating of the Quaternary glaciations in the southern Shaluli Mountain on the Southeastern Tibetan Plateau. Sci. China, Ser. D, Earth Sci. 49 (12), 1291–1298.

Wang, J., Pan, B., Zhang, G., Cui, H., Cao, B., Geng, H., 2013. Late Quaternary glacial chronology on the eastern slope of Gongga Mountain, eastern Tibetan Plateau, China. Sci. China 56, 354–365. https://doi.org/10.1007/s11430-012-4514-0.

Xu, L., Zhou, S., 2009. Quaternary glaciations recorded by glacial and fluvial landforms in the Shaluli Mountains, southeastern Tibetan Plateau. Geomorphology 103, 268–275.

Yu, H., Wang, L., Yang, R., Yang, M., Gao, R., 2018. Temporal and spatial variation of precipitation in the Hengduan Mountains region in China and its relationship with elevation and latitude. Atmos. Res. 213, 1–16. https://doi.org/10.1016/j.atmosres.2018.05.025.

Zhang, Z., Wang, J., Xu, X., Bai, S., Chang, Z., 2015. Cosmogenic ^{10}Be and ^{26}Al chronology of the last glaciation of the palaeo-Daocheng Ice Cap, southeastern Qinghai–Tibetan Plateau. Acta Geol. Sin. 89, 575–584.